Liang, A.; Rahman, S.; Rodriguez-Hernandez, P.; Muñoz, A.; Manjón, F.; Nenert, G.; Errandonea, D. (2020). High-pressure Raman study of Fe(IO3)3: Soft-mode behavior driven by coordination changes of iodine atoms. The Journal of Physical Chemistry C. 124(39):21329-21337. https://doi.org/10.1021/acs.jpcc.0c06541

High-pressure Raman study of $Fe(IO_3)_3$: Soft-mode behavior driven by coordination changes of iodine atoms

Akun Liang[1], Saqib Rahman[2], Placida Rodriguez-Hernandez[3], Alfonso Muñoz[3], Francisco Javier Manjón[4], Gwilherm Nenert[5], and Daniel Errandonea[1]

[1]Departamento de Física Aplicada - ICMUV - MALTA Consolider Team, Universitat de València, c/Dr. Moliner 50, 46100 Burjassot (Valencia), Spain

[2]Center for High Pressure Science and Technology Advanced Research, Shanghai 201203, China

[3]Departamento Física, Malta Consolider Team, and Instituto de Materiales y Nanotecnología, Universidad de La Laguna, 38206 La Laguna, Tenerife, Spain

[4]Instituto de Diseño para la Fabricación y Producción Automatizada, MALTA-Consolider Team, Universitat Politècnica de València, 46022 Valencia, Spain

[5]Malvern Panalytical B.V., Lelyweg 1, 7602 EA Almelo, The Netherlands

ABSTRACT: We report high-pressure Raman spectroscopy studies of $Fe(IO_3)_3$ up to nearly 21 GPa that have been interpreted with the help of density-functional theory calculations, that include the calculation of phonon dispersion curves and elastic constants at different pressures. Zero-pressure Raman-active mode frequencies and their pressure dependences have been determined. Modes have been assigned and correlated to atomic movements with the help of calculations. Interestingly, in the high-frequency region there are several modes that soften under compression. These modes have been identified as internal vibrations of the IO_3 coordination polyhedron. Their unusual behavior is a consequence of the changes induced by pressure in the coordination sphere of iodine, which gradually change from a three-fold to almost six-fold coordination under compression. The coordination change is favored by the decrease of the stereoactivity of the iodine lone electron pair, so that likely real six-fold coordination is attained after a first-order phase transition previously reported to occur above 21 GPa. The strong non-linear behavior found in Raman-active modes as well as in theoretically calculated elastic constants has been discovered to be related to the occurrence of two previously unreported isostructural phase transitions at 1.5-2.0 GPa and 5.7-6.0 GPa as shown by dynamic instabilities close to the Brillouin zone center.

TOC IMAGE

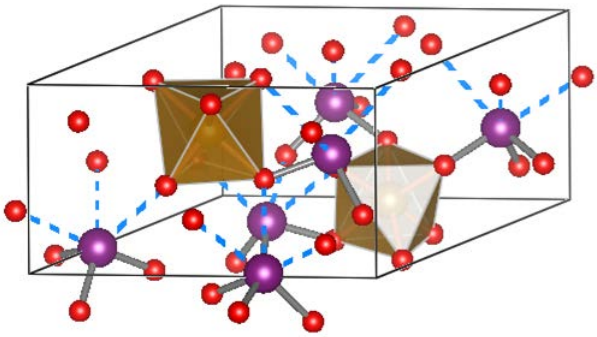

KEYWORDS: $Fe(IO_3)_3$, Phase transition, High pressure, Raman spectroscopy, soft modes

Metal iodates usually show asymmetric coordination geometry due to the presence of lone electron pairs (LEPs) in the iodine atom. Consequently, they can form a diversity of unusual structures and many of them have multiple promising properties or applications, such as a large second harmonic generation coefficient materials,[1–4] chiral materials with second-order nonlinear optical activity in the visible, near and mid-IR ranges,[5] and barocaloric materials.[6]

Of particular interest are compounds with composition $M(IO_3)_3$, with M being a trivalent metal atom and iodine (I) being a pentavalent atom. These metal iodates show a diversity of unusual crystalline structures due to the asymmetric coordination geometry produced by the iodine LEP. A feature of these compounds is that IO_3 units do not form planar triangles, like in borate (BO_3) or carbon trioxide (CO_3) units. Instead, IO_3 units are not planar and have a pyramidal form with three O atoms in the corners of the base and the iodine atom in the top corner of the pyramid. This unit can be seen in Fig. 1, where the crystal structure of $Fe(IO_3)_3$ is schematically represented. In fact, the polyhedron around I could be described as IO_3E tetrahedron, where E is the iodine LEP. Therefore, iodine can be considered as four-fold coordinated if we take into account the LEP, with iodine sitting in the center of a distorted tetrahedron where the oxygen atoms are occupying three corners, and the fourth one is occupied by the lone pair of electrons of the iodine atom. It should be noted that the I-O bond distance in the IO_3E unit is of the order of 1.9 Å, while the I-O distances to the three second-next oxygen neighbors are between 2.55 and 2.95 Å (see Fig. 1). We will show that these atoms become relevant at high pressure (HP) to increase the coordination of I atoms and explain the changes observed in the vibrational properties of $Fe(IO_3)_3$.

It is well-known that HP modifies interatomic distances, leading to changes in the physical properties of materials. This has contributed to improve the properties of materials and

to several discoveries that have impacted physics, chemistry, and materials sciences. Among transition-metal iodates, such studies have been carried out only in $Fe(IO_3)_3$.[7] This material was studied by powder x-ray diffraction (XRD), infrared (IR) spectroscopy, and density-functional theory (DFT) simulations. It undergoes a first-order phase transition at 22 GPa, with a volume change and an abrupt change of the c/a axial ratio. The phase transition is triggered by changes in the coordination of iodine atoms, which is driven by the decrease of the stereoactivity of the iodine LEP. DFT calculations have proposed the occurrence of an unusual softening of vibrational modes associated with internal vibrations of the IO_3 molecule. However, this hypothesis has not been confirmed by Raman experiments yet, which have been only reported at ambient conditions.[8,9]

In this work, we will explore the proposed phonon-softening phenomenon by HP Raman spectroscopy (RS), which will be analyzed with the help of *ab initio* DFT calculations. We have performed high-pressure-RS (HP-RS) experiments up to 21 GPa to avoid the influence of precursor effects of the first-order phase transition that has been reported to occur at 22 GPa. Combining experimental and theoretical results, we will propose by the first time a tentative symmetry assignment for Raman modes of $Fe(IO_3)_3$ and discuss the nature of the soft phonons. In particular, we have found evidence of the occurrence of two subtle isostructural phase transitions (IPTs), which were not detected by previous studies.

Before presenting and discussing our results we will briefly describe the crystal structure of $Fe(IO_3)_3$ which is shown in Fig. 1. The description of the structure is relevant for the discussion of results here reported. In Fig. 1, it can be seen that the structure is formed by FeO_6 octahedral units connected by isolated IO_3 trigonal pyramids which deviate from the ideal 3m point symmetry because the lone pair takes up a larger region of space than do the single I-O

bonds. In the figure, we have included the bonds corresponding to the IO_3 coordination polyhedron and dashed lines indicating the three second-neighbor O atoms, which become relevant under compression.

We will start discussing the Raman spectra near ambient conditions. Our spectrum at 0.5 GPa, the lowest measured pressure (shown in Fig. 2), is very similar to those reported in the literature.[8,9] As it can be observed, the Raman-active modes are distributed in two isolated regions. One region for wavenumbers smaller than 500 cm^{-1} and another for wavenumbers larger than 650 cm^{-1}, with a phonon gap between the two regions. The strongest mode is located at 792 cm^{-1}. Along the paper, we will show that the high-frequency modes are linked to I-O vibrations. In particular, they are internal modes of IO_3 units.

For $Fe(IO_3)_3$, group theory predicts thirty-seven Raman-active modes ($12A + 12E_1 + 13E_2$). In previous studies,[8,9] Ristic *et al.* measured seventeen modes and Bushiri *et al.* measured fourteen modes. In our experiments, we have measured twenty modes. The Raman-active modes are summarized in Table 1, where they have been given a superindex to number them in order of increasing frequency. It can be seen that there is a good agreement between the frequencies reported in different experiments.

DFT calculated frequencies of $Fe(IO_3)_3$ are also reported in Table 1. DFT calculations give a good description of experimentally-observed Raman-active mode frequencies, with differences being smaller than 10%, which is typical for most oxides.[10] In particular, the mode frequencies of $Fe(IO_3)_3$ in the low-frequency region are slightly underestimated by our PBEsol+U calculations, as happens in many other oxides.[10] On the other hand, the calculated high-frequency modes have an offset of nearly 60 cm^{-1} with respect to experiments. The

comparison of frequencies and their pressure dependences (to be discussed below in relation to Fig. 3) allowed us to propose a tentative assignment of the experimentally-observed Raman-active modes. The symmetry of the different modes is included in Table 1.

According to our mode assignment, the strongest Raman-active mode, located at wavenumber 792 cm^{-1} (A^{11} mode in Table 1), can be identified as an internal symmetric stretching vibration of O atoms against the I atom inside IO_3 units (see Fig. S1 in the Supplementary Information (SI)) and calculated to be at 729.2 cm^{-1} in Table 1. Notice that DFT not only describe properly Raman-active modes but also IR-active modes, already reported,[7] and their pressure dependence.

Interestingly, in many metal iodates with different compositions, the strongest Raman-active mode is always located in the 730 – 800 cm^{-1} region. In $Ni(IO_3)_2$, $Mn(IO_3)_2$, $Co(IO_3)_2$, and $Zn(IO_3)_2$, the strongest Raman-active mode is in the 763-782 cm^{-1} range.[11] In $Al(IO_3)_3$, $Ga(IO_3)_3$, and $In(IO_3)_3$, it is in the 730 - 800 cm^{-1} range.[12] Finally, in KIO_3, the strongest mode[13] is at 748 cm^{-1}. All these iodates have in common that in their structure iodine atoms form IO_3 trigonal pyramids with very short I-O bond distances. Based on this fact, it has been generally assumed that the strongest Raman-active mode of each compound is an internal symmetric stretching I-O vibration inside the IO_3 unit. In the case of $Fe(IO_3)_3$, we support this conclusion by calculating the atomic motions associated with those modes (see Fig. S1). This fact will be discussed in more detail when presenting the HP results. The three Raman-active modes (E_1[12], A^{12} and E_2[13]) with higher frequencies than the symmetric stretching mode correspond to asymmetric stretching I-O vibrations inside the IO_3 unit (see Figs. S2, S3, and S4 in Supplementary Material).

We will start now discussing the HP behavior of the Raman spectra in $Fe(IO_3)_3$. In Fig. 2, we show Raman spectra at different pressures. They show a monotonous behavior with no abrupt changes up to 21 GPa, indicating that a first-order transition is not happening in this pressure range. This is in good agreement with results from previous XRD measurements.[7] Previous infrared spectroscopy studies located the transition at 15 GPa.[7] The lower transition pressure observed in these experiments is due to the use of a less hydrostatic medium in IR experiments (CsI) than in present Raman and previous XRD experiments (silicone oil).[7,10,14,15] However, as we will discuss next, there are modes showing strong non-linear pressure dependences and soft-mode behaviors that suggest possible continuous transitions as we will discuss next. All changes observed in the RS spectrum under compression are reversible as can be seen in Fig. 2 in the top RS spectrum measured after decompression. Note that at 10 GPa, there are two peaks near 300 cm^{-1} that overlap. This causes an apparent increase in intensity at this frequency. In Fig. 2, a pressure-induced closing of the phonon gap can be also noticed. This fact is mainly caused by the hardening of modes below 450 cm^{-1} and the softening of all the measured high-frequency modes. Therefore, the closing of the phonon gap, evident in Fig. 3, where we have plotted the pressure dependence of the experimental and theoretical Raman-active modes, also suggests an increase of I coordination.

Experimental and theoretical zero-pressure frequencies, pressure coefficients, and Grüneissen parameters show a relatively good agreement, as can be seen in Fig. 3 and in Table 1. In the figure, DFT results are shown only up to 12 GPa, because they underestimate the transition pressure of the first-order transition, as discussed in Ref. 7. Therefore, for consistency DFT results are compared with experiments only for the pressures below the theoretical first-order phase transition. As observed in Fig. 3, many Raman-active modes show anomalous

pressure dependences. Not only there are high-frequency soft modes but also there are many modes in the low- and high-frequency region that show an S-like non-linear pressure dependence that will be commented later. Consequently, zero-pressure coefficients in Table 1 have been obtained using the pressure range where the frequency dependence is linear with pressure, near 0 GPa, and Grüneisen parameters have been calculated using the bulk moduli given in the caption of Table 1. In Figs. 2 and 3, it can be seen that there is a progressive closing of the phonon gap with increasing pressure that suggests the existence of a close first-order phase transition above 21 GPa; i.e. consistent with XRD measurements.[7] Additionally, in the high-frequency region all the modes of $Fe(IO_3)_3$ have a soft-mode behavior, at least between 0 and 2 GPa. Using J-ICE we have identified that the high-frequency modes mainly correspond to symmetric and asymmetric I-O stretching vibrations inside the IO_3 units (see Figs. S1 to S4 as examples). As shown in Fig. 3, DFT not only supports the existence of soft modes but also provides a qualitatively good description for the pressure dependence of most observed modes. Note that, for high-frequency modes, theoretical calculations describe nicely the pressure dependence of experimental mode frequencies when an upward shift of 60 cm^{-1} is applied to calculated frequencies.

Interestingly, we have found that one of the experimental soft modes of $Fe(IO_3)_3$ is the strongest mode at 792 cm^{-1} that we have tentatively attributed to the A^{11} mode (with a calculated frequency of 729.2 cm^{-1}). The observed mode softening of the high-frequency modes can be correlated to the pressure-induced increase of two of the short I-O bond distances (see Fig. 4), which is expected to reduce the restoring force of stretching vibrations. According to our calculations, iodine atoms are three-fold coordinated at room pressure; however, as pressure increases coordination becomes first four-fold (at least above 5.7 GPa) and then gradually approach a six-fold coordination (see Fig. 4) becoming six at the phase transition at 22 GPa.[7]

This can be explained by the progressive reduction of the iodine LEP stereoactivity with increasing pressure, as found in a number of heavy pnictogen (As, Sb, and Bi) compounds with a strong LEP stereoactivity at room pressure, like α-Sb_2O_3,[16–18] β-Bi_2O_3,[19,20] isostructural Sb_2S_3, Sb_2Se_3, and Bi_2S_3 compounds,[21] α-As_2Te_3,[22] $SbPO_4$,[23] and As_2S_3.[24]

Under a harmonic approximation, it can be assumed as a first approximation that the force constant, k, of the internal phonons of IO_3 is a function of $(d_{I-O})^{-3}$, where d_{I-O} is the average I-O bond distance.[25] Since the frequency of a stretching mode is proportional to the square root of the force constant and inverse proportional to the square root of the reduced mass, μ, of the bond, $\omega = (k/\mu)^{1/2}$, we have that $\omega^{-2/3}$ should have a linear dependence on the average I-O bond distance. Using the results of our calculations, we have correlated the theoretical frequencies of the soft modes with the theoretical average I-O bond distance in IO_3 units (see Fig. 5). There it can be seen that indeed there is a clear linear relationship between the $\omega^{-2/3}$ and the calculated average I-O bond distance for the soft high-frequency modes. Thus, the decrease of the phonon frequencies is a consequence of the slight enlargement of the three shortest I-O distances in order to accommodate additional O atoms around iodine as pressure increases.

It is noteworthy that the average distance of the three short I-O bonds of the IO_3 unit increases slightly under compression due to the changes induced by pressure in the crystal structure of $Fe(IO_3)_3$.[7] Simultaneously, second-neighbor I-O distances above 2.5 Å show a notably decrease at HP (see Fig. 4). Therefore, these O atoms enter progressively into the coordination sphere of iodine atoms and induce changes in the coordination of I atoms. We believe the enlargement of the short I-O bonds under compression is responsible for the softening of most high-frequency modes and is a consequence of a charge transfer from the short

I-O bonds to the large I-O bonds in order to increase the iodine coordination. Such an increase of the bond distance and decrease of the bond charge has been recently observed in As_2S_3[24] and has been related to the novel phenomena of "metavalent" bonding; i.e. the observation of a new-type of chemical bonding intermediate between covalent and metallic bonding and characterized by bonds with less than two electrons per bond.[26,27] In some oxides with strong LEP stereoactivity at room pressure, this behavior has been related to the existence of a unusual IPTs, like in α-Sb_2O_3[16–18] and β-Bi_2O_3.[19,20]

We will present now evidence supporting the existence of subtle IPTs in $Fe(IO_3)_3$. Such transitions were not detected by previous XRD studies because of this subtle phase transitions involve only continuous changes in the crystal structure, with no discontinuities in the unit-cell parameters or atomic positions. In contrast, RS experiments, sensing local properties, as the vibrations are, are more sensitive for detecting such subtle transitions. We have found evidence for the two IPTs not only from the pressure dependence of phonons and bond distances, but also from the analysis of atomic positions and elastic constants that correlate with changes in lattice parameters at HP. A detailed analysis of all this information places the transitions, near 1.5-2.0 and 5.7-6.0 GPa. For the sake of briefness, we present the evidence for the two IPTs in Figs. S5 to S10 of the SI. These figures show the theoretical pressure dependence of the unit-cell parameters and free atomic parameters of $Fe(IO_3)_3$. In particular, the two IPTs, marked by the vertical dashed lines in those figures, can explain the strong non-linear S-like behavior of a number of parameters of $Fe(IO_3)_3$; for instance, the z coordinate of the Fe atom. Additional support for the two IPTs near 1.5 and 5.7 GPa comes from the pressure dependence of the elastic constants, which is shown in Fig. 6. In particular, at 1.7 GPa there is a clear jump of C_{33}, C_{66}, C_{12}, C_{13}. Such changes are indicative of the occurrence of phase transitions.[28–30] At 5.7 GPa there

are also changes in the elastic constant, they are less evident that at 1.7 GPa; but there are detectable changes in the pressure dependence of C_{13} and C_{33} as can be seen in Fig. 6.

In order to understand the nature of the two IPTs without change of volume, we have calculated the phonon dispersion curves of $Fe(IO_3)_3$ at 0, 1.5, 5.7, and 7.5 GPa, which are shown in Fig. 7. As observed, the phonon dispersion curves show small dynamic instabilities (negative frequencies) near the Γ-point at 1.5 and 5.7 GPa that are not observed either at 0 or at 7.5 GPa. Consequently, we can conclude that the two IPTs observed in $Fe(IO_3)_3$ are of a similar nature as the one of tetragonal β-Bi_2O_3[19,20] and perhaps also in α-Sb_2O_3.[16–18]

Additional support to the existence of two IPTs in $Fe(IO_3)_3$ comes from the study of phonon lifetime change with pressure. In the case of Raman spectroscopy, the full width at half maximum (FWHM) is related inversely to the phonon lifetime. The pressure dependence of the FWHM of two modes of $Fe(IO_3)_3$, which do not overlap with other modes, is shown in Fig. 8. It is evident from the that the line width of the mode with wavenumber 400 cm^{-1} increases substantially with pressure beyond 2 GPa. On the other hand, the mode with wavenumber 792 cm^{-1} as a sharp change in the pressure evolution of the line width at 6 GPa. Such changes are typical of IPT transitions.[18-22] We think that the fact that they take place at the same pressure that changes in pressure dependence of phonons, bond-distances, and elastic constants is not a mere coincidence, but another evidence of the occurrence of IPTs in $Fe(IO_3)_3$. Additional changes are observed in the behavior of phonons FWHM around 15 – 20 GPa, but they are related to precursor effects of the first-order transition previously reported at 22 GPa.

Summing up, both Raman experiments and DFT calculations support that there are soft-modes in $Fe(IO_3)_3$ which are related to the increase of the three short I-O bonds with pressure.

The short I-O bonds increase while the second-neighbor I-O bonds decrease with pressure. Moreover, the non-linear S-like behavior of several Raman-active modes (also of several IR-active modes),[7] as well as of some elastic constants can be explained by the occurrence of two IPTs around 1.5-2.0 and 5.7-6.0 GPa. The two IPTs are clearly related to changes in the behavior of lattice parameters and free atomic positions.

The formation of additional I-O bonds at HP in metal iodates has important consequences of the behavior of phonons under compression.[31] Therefore, the present discovery of continuous IPTs in a metal iodate, like $Fe(IO_3)_3$, opens the door to interesting findings in this family of compounds at HP. In particular, we have noticed that in KIO_3 also two internal stretching modes of the IO_3 unit are soft modes.[13] This compound undergoes a phase transition at 5 GPa. It would be not surprising that the observed soft modes in KIO_3 could be related to a collective instability which makes the crystal structure unstable, thus triggering a phase transition.[32,33] This suggests that the triggering of phase transitions by soft modes could be a common feature of metal iodates.

In conclusion, The lattice dynamics of $Fe(IO_3)_3$ has been studied up to 21 GPa, within the range of stability of the low-pressure hexagonal phase, by means of Raman spectroscopy measurements, which have been interpreted using density-functional theory calculations. Our measurements and calculations evidence a progressive decrease of the phonon gap and the softening of most high-frequency vibrational modes at least up to 2 GPa. The frequency, pressure dependence, and symmetry of the different modes have been determined. The soft modes in the high-frequency region are related to internal I-O vibrations of IO_3 units. Among them, we include the symmetric stretching I-O vibration of IO_3 units, which is the strongest Raman-active mode. The soft mode behavior is proposed to be connected with the increase of the shortest I-O

bond distances due to a gradual increase of the iodine coordination that leads to a decrease of the short I-O bond forces due to a charge transfer to long I-O distances. The non-linear S-like behavior of a number of experimental and theoretical Raman-active modes, as well as other physical properties, can be explained by the existence of two isostructural phase transitions at 1.5-2.0 and 5.7-6.0 GPa which occur without a volume change and only a change in volume compressibility. Our results have been compared with result from other metal iodates in order to try to find general features in the iodate family. The present discovery of unusual isostructural phase transitions in a metal iodate, like $Fe(IO_3)_3$, and their relationship to soft modes open the door to interesting findings in the iodate family of compounds under compression and invite to revisit the high pressure behavior of iodine-based compounds, like KIO_3.

METHODS

Samples: For the study of $Fe(IO_3)_3$, we used the same sample used in our previous x-ray diffraction (XRD) and infrared (IR) studies[7] that was prepared by a co-precipitation technique. A description of the sample preparation method can be found in Ref. 7. The purity of the sample and crystal structure was confirmed by XRD measurements.[7]

High-pressure generation: We performed HP-RS measurements at room temperature up to 21 GPa using silicone oil as a pressure-transmitting medium (PTM)[14,15] to avoid the hydration of the metal iodates,[1] and the ruby fluorescence scale as our pressure gauge.[34] For these studies, samples, ruby chips and the PTM were loaded in the 200-μm diameter hole of a pre-indented steel gasket inside a diamond-anvil cell (DAC). We made a careful loading of materials inside the DAC to avoid both sample hydration and sample bridging between diamond anvils.[35]

Raman spectroscopy: HP-RS measurements, with a fixed time of 20 s, were performed using an inVia Renishaw Raman spectrometer system with a 5× magnification objective. A laser wavelength of 532 nm and a grating of 2400 lines·mm^{-1}, provided a spectral resolution better than 2 cm^{-1}.

Overview of the calculations: DFT calculations were used for the interpretation of experiments and mode assignment. Total-energy and phonon calculations as a function of pressure for $Fe(IO_3)_3$ were previously published by part of the coauthors of this work.[7] Such calculations were performed using the Vienna *ab initio* simulations package (VASP) within the generalized gradient approximation (GGA) with the PBE for solids (PBEsol) functionals. The Hubbard potential, U, was also used (Ueff = 5.4 eV) to account for the strong correlation between the electrons in the d shell, as we previously did to explain XRD and IR results.[7] After optimizing the crystal structure at different pressures, phonon frequencies and phonon dispersion curves were calculated using the direct force method. The elastic constants were calculated using density functional perturbation theory. Thanks to DFT calculations we have been able to identify atomic motions associated with phonons using the J-ICE software.[36]

ASSOCIATED CONTENT

Supporting Information.

Figures showing atomic vibrations of Raman modes, calculated pressure dependence of unit-cell parameters and atomic positions are included in the Supporting Information.

Corresponding Author

*E-mail: daniel.errandonea@uv.es

Author Contributions

The manuscript was written through contributions of all authors. All authors have given approval to the final version of the manuscript.

Funding Sources

Grants No. grant MAT2016-75586-C4-1/2/3-P, PID2019-106383GB-C41/42/43, RED2018-102612-T (MALTA Consolider-Team Network), and Prometeo/2018/123 (EFIMAT) from the Spanish Ministerio de Ciencia, Innovación y Universidades, the Spanish Research Agency (AEI), the Generalitat Valenciana, and the European Fund for Regional Development (ERDF, FEDER).

Notes

The authors declare no competing financial interest.

ACKNOWLEDGMENT

This work was supported by the Spanish Ministry of Science, Innovation and Universities under grant MAT2016-75586-C4-1/2/3-P, PID2019-106383GB-C41/42/43, and RED2018-102612-T (MALTA Consolider-Team Network) and by Generalitat Valenciana under grant Prometeo/2018/123 (EFIMAT). A. L. and D. E. would like to thank the Generalitat Valenciana for the Ph.D. fellowship GRISOLIAP/2019/025).

REFERENCES

(1) Nassau, K.; Shiever, J. W.; Prescott, B. E. Transition Metal Iodates. I. Preparation and Characterization of the 3d Iodates. *J. Solid State Chem.* **1973**, *7*, 186–204.

(2) Jansen, M. Zur Kistallstruktur von FeJ_3O_9. *J. Solid State Chem.* **1976**, *17*, 1–6.

(3) Hu, C. L.; Mao, J. G. Recent Advances on Second-Order NLO Materials Based on Metal Iodates. *Coord. Chem. Rev.* **2015**, *288*, 1–17.

(4) Hebboul, Z.; Galez, C.; Benbertal, D.; Beauquis, S.; Mugnier, Y.; Benmakhlouf, A.; Bouchenafa, M.; Errandonea, D. Synthesis, Characterization, and Crystal Structure Determination of a New Lithium Zinc Iodate Polymorph $LiZn(IO_3)_3$. *Crystals* **2019**, *9*, 464.

(5) Bergman, J. G.; Boyd, G. D.; Ashkin, A.; Kurtz, S. K. New Nonlinear Optical Materials: Metal Oxides with Nonbonded Electrons. *J. Appl. Phys.* **1969**, *40*, 2860–2863.

(6) Sagotra, A. K.; Errandonea, D.; Cazorla, C. Mechanocaloric Effects in Superionic Thin Films from Atomistic Simulations. *Nat. Commun.* **2017**, *8*, 963.

(7) Liang, A.; Rahman, S.; Saqib, H.; Rodriguez-Hernandez, P.; Munoz, A.; Nenert, G.; Yousef, I.; Popescu, C.; Errandonea, D. First-Order Isostructural Phase Transition Induced by High-Pressure in Fe(IO 3) 3. *J. Phys. Chem. C* **2020**, *124* (126), 8669–8679.

(8) Ristić, M.; Musić, S.; Ivanda, M. A Study of the Thermal Stability of $Fe(IO_3)_3$ by ^{57}Fe Mossbauer, FT- IR and Raman Spectroscopies. *J. Mol. Struct.* **1999**, *480–481*, 637–640.

(9) Bushiri, M. J.; Kochuthresia, T. C.; Vaidyan, V. K.; Gautier-Luneau, I. Raman Scattering Structural Studies of Nonlinear Optical $M(IO_3)_3$(M=Fe, Ga, α-In) and Linear Optical β-$In(IO_3)_3$. *J. Nonlinear Opt. Phys. Mater.* **2014**, *23*, 1–9.

(10) Errandonea, D.; Muñoz, A.; Rodríguez-Hernández, P.; Gomis, O.; Achary, S. N.; Popescu, C.; Patwe, S. J.; Tyagi, A. K. High-Pressure Crystal Structure, Lattice Vibrations, and Band Structure of $BiSbO_4$. *Inorg. Chem.* **2016**, *55*, 4958–4969.

(11) Kochuthresia, T. C.; Gautier-Luneau, I.; Vaidyan, V. K.; Bushiri, M. J. Raman and Ftir Spectral Investigations of Twinned $M(IO_3)_2$ (M = Mn, Ni, Co, AND Zn) Crystals. *J. Appl. Spectrosc.* **2016**, *82*, 941–946.

(12) Ngo, N.; Kalachnikova, K.; Assefa, Z.; Haire, R. G.; Sykora, R. E. Synthesis and Structure of In(IO3)3 and Vibrational Spectroscopy of $M(IO3)_3$ (M=Al, Ga, In). *J. Solid State Chem.* **2006**, *179*, 3824–3830.

(13) Shen, Z. X.; Wang, X. B.; Tang, S. H.; Li, H. P.; Zhou, F. High Pressure Raman Study and Phase Transitions of KIO_3 Non-Linear Optical Single Crystals. *Rev. High Press. Sci. Technol. No Kagaku To Gijutsu* **1998**, *7*, 751–753.

(14) Klotz, S.; Chervin, J. C.; Munsch, P.; Le Marchand, G. Hydrostatic Limits of 11 Pressure Transmitting Media. *J. Phys. D. Appl. Phys.* **2009**, *42*, 075413.

(15) Errandonea, D.; Meng, Y.; Somayazulu, M.; Häusermann, D. Pressure-Induced → ω Transition in Titanium Metal: A Systematic Study of the Effects of Uniaxial Stress. *Phys. B Condens. Matter* **2005**, *355*, 116–125.

(16) Zhang, Z.; Sui, Z.; Hu, S.; Chen, H.; Gao, C.; Su, H.; Rahman, A.; Dai, R.; Wang, Z.; Zheng, X. Laser Effects on Phase Transition for Cubic Sb_2O_3 Microcrystals under High Pressure. *J. Mater. Chem. C* **2017**, *5*, 5451–5457.

(17) Zhao, Z.; Zeng, Q.; Zhang, H.; Wang, S.; Hirai, S.; Zeng, Z.; Mao, W. L. Structural Transition and Amorphization in Compressed α-Sb_2O_3. *Phys. Rev. B - Condens. Matter Mater. Phys.* **2015**, *91*, 184112.

(18) Pereira, A. L. J.; Gracia, L.; Santamaría-Pérez, D.; Vilaplana, R.; Manjón, F. J.; Errandonea, D.; Nalin, M.; Beltrán, A. Structural and Vibrational Study of Cubic Sb_2O_3 under High Pressure. *Phys. Rev. B - Condens. Matter Mater. Phys.* **2012**, *85*, 174108.

(19) Pereira, A. L. J.; Gomis, O.; Sans, J. A.; Contreras-García, J.; Manjón, F. J.; Rodríguez-Hernández, P.; Muñoz, A.; Beltrán, A. β-Bi_2O_3 under Compression: Optical and Elastic Properties and Electron Density Topology Analysis. *Phys. Rev. B* **2016**, *93*, 224111.

(20) Pereira, A. L. J.; Sans, J. A.; Vilaplana, R.; Gomis, O.; Manjón, F. J.; Rodríguez-Hernández, P.; Muñoz, A.; Popescu, C.; Beltrán, A. Isostructural Second-Order Phase Transition of β-Bi_2O_3 at High Pressures: An Experimental and Theoretical Study. *J. Phys. Chem. C* **2014**, *118*, 23189–23201.

(21) Ibáñez, J.; Sans, J. A.; Popescu, C.; López-Vidrier, J.; Elvira-Betanzos, J. J.; Cuenca-Gotor, V. P.; Gomis, O.; Manjón, F. J.; Rodríguez-Hernández, P.; Muñoz, A. Structural, Vibrational, and Electronic Study of Sb_2S_3 at High Pressure. *J. Phys. Chem. C* **2016**, *120*, 10547–10558.

(22) Cuenca-Gotor, V. P.; Sans, J. A.; Ibáñez, J.; Popescu, C.; Gomis, O.; Vilaplana, R.; Manjón, F. J.; Leonardo, A.; Sagasta, E.; Suárez-Alcubilla, A.; et al. Structural, Vibrational, and Electronic Study of α-As_2Te_3 under Compression. *J. Phys. Chem. C* **2016**, *120*, 19340–19352.

(23) Pereira, A. L. D. J.; Santamariá-Pérez, D.; Vilaplana, R.; Errandonea, D.; Popescu, C.; Da Silva, E. L.; Sans, J. A.; Rodríguez-Carvajal, J.; Munõz, A.; Rodríguez-Hernández, P.; et al. Experimental and Theoretical Study of $SbPO_4$ under Compression. *Inorg. Chem.* **2020**, *59*, 287–307.

(24) Cuenca-Gotor, V. P.; Sans, J. Á.; Gomis, O.; Mujica, A.; Radescu, S.; Muñoz, A.; Rodríguez-Hernández, P.; Da Silva, E. L.; Popescu, C.; Ibañez, J.; et al. Orpiment under Compression: Metavalent Bonding at High Pressure. *Phys. Chem. Chem. Phys.* **2020**, *22*, 3352–3369.

(25) Bucknum, M. Compressibility of Calcium Nitride to 137 Kb. *Nat. Preced.* **2008**. DOI: 10.1038/npre.2008.1771.4.

(26) Wuttig, M.; Deringer, V. L.; Gonze, X.; Bichara, C.; Raty, J. Y. Incipient Metals: Functional Materials with a Unique Bonding Mechanism. *Adv. Mater.* **2018**, *30*, 1803777.

(27) Raty, J. Y.; Schumacher, M.; Golub, P.; Deringer, V. L.; Gatti, C.; Wuttig, M. A Quantum-Mechanical Map for Bonding and Properties in Solids. *Adv. Mater.* **2019**, *31*, 1806280.

(28) Boccara, N. Second-Order Phase Transitions Characterized by a Deformation of the Unit Cell. *Ann. Phys. (N. Y).* **1968**, *47*, 40–64.

(29) Errandonea, D. Landau Theory Applied to Phase Transitions in Calcium Orthotungstate and Isostructural Compounds. *EPL* **2007**, *77*, 56001.

(30) Tröster, A.; Schranz, W.; Ehsan, S.; Belbase, K.; Blaha, P. Symmetry-Adapted Finite Strain Landau Theory Applied to $KMnF_3$. *Crystals* **2020**, *10*, 124.

(31) Monteseguro, V.; Errandonea, D.; Achary, S. N.; Sans, J. A.; Manjón, F. J.; Gallego-Parra, S.; Popescu, C. Structural Characterization of Aurophilic Gold(I) Iodide under High Pressure. *Inorg. Chem.* **2019**, *58*, 10665–10670.

(32) Errandonea, D.; Pellicer-Porres, J.; Pujol, M. C.; Carvajal, J. J.; Aguiló, M. Room-Temperature Vibrational Properties of Potassium Gadolinium Double Tungstate under Compression up to 32 GPa. *J. Alloys Compd.* **2015**, *638*, 14–20.

(33) Liu, J.; Shen, Z.; Zhang, Y.; Yin, X.; He, S. The P-T Phase Diagram of Lithium Iodate ($LiIO_3$) up to 40 Kbars. *acta phys. sin* **1983**, *32*, 118–123.

(34) Mao, H. K.; Xu, J.; Bell, P. M. Calibration of the Ruby Pressure Gauge to 800 Kbar under Quasi-Hydrostatic Conditions. *J. Geophys. Res.* **1986**, *91*, 4673–4676.

(35) Errandonea, D.; Muñoz, A.; Gonzalez-Platas, J. Comment on "High-Pressure x-Ray Diffraction Study of YBO_3/Eu^{3+}, $GdBO_3$, and $EuBO_3$: Pressure-Induced Amorphization in $GdBO_3$" [J. Appl. Phys. 115, 043507 (2014)]. *J. Appl. Phys.* **2014**, *115*, 216101.

(36) Canepa, P.; Hanson, R. M.; Ugliengo, P.; Alfredsson, M. J-ICE: A New Jmol Interface for Handling and Visualizing Crystallographic and Electronic Properties. *J. Appl. Crystallogr.* **2011**, *44*, 225–229.

Table 1. Theoretical and experimental zero-pressure frequencies, ω, pressure coefficients, dω/dP, and Grüneisen parameters, γ, of Raman-active modes of $Fe(IO_3)_3$. In fact, our experimental frequencies correspond to 0.5 GPa. Raman-active (R) or both Raman- and IR-active (RI) are indicated. Results of previous experiments[8,9] have been also included for comparison. To calculate the Grüneisen parameters, we have used the theoretical bulk modulus (36 GPa) for calculations and the experimental bulk modulus (55 GPa) for experiments.[7]

	Theory			Experiment				
Mode	ω_0 [a] (cm^{-1})	$d\omega/dP$ [a] (cm^{-1}/GPa)	γ[a]	ω_0 [a] (cm^{-1})	$d\omega/dP$ [a] (cm^{-1}/GPa)	γ[a]	ω_0[b] (cm^{-1})	ω_0[c] (cm^{-1})
A^1(RI)	57.3	-0.08	-0.05					55
E_1^1(RI)	65.6	3.10	1.70					
E_2^1(R)	79.8	1.24	0.56					
E_2^2(R)	89.6	5.21	2.09				86	85
A^2(RI)	112.3	4.88	1.56	112	2.44	1.20		110
E_1^2(RI)	119.8	2.48	0.75	121	1.78	0.81	125	125
A^3(RI)	126.1	1.85	0.53					
E_2^3(R)	131.8	5.57	1.52	131	3.57	1.50		
E_1^3(RI)	165.4	3.96	0.86	175	0.70	0.22	166	165
E_2^4(R)	172.3	6.65	1.39					
E_2^5(R)	194.5	4.49	0.83					
E_1^4(RI)	202.2	6.16	1.10					
A^4(RI)	212.7	2.53	0.43	212	2.76	0.72		205
E_1^5(RI)	219.4	9.30	1.53					
E_2^6(R)	223.5	5.17	0.83	230	4.27	1.02	223	225
A^5(RI)	239.8	6.48	0.97	237	6.76	1.57		
E_2^7(R)	245.3	7.99	1.17					
E_1^6(RI)	269.8	4.83	0.64					
A^6(RI)	270.7	7.35	0.98	274	7.14	1.43	266	265
A^7(RI)	291.7	1.88	0.23	316	0.65	0.11	320	315
E_1^7(RI)	316.5	4.51	0.51	334	1.36	0.22		
E_2^8(R)	334.2	2.90	0.31	353	1.78	0.28	350	350

E_1^8(RI)	382.5	4.06	0.38					
E_2^9(R)	385.5	6.06	0.57					
A^8(RI)	391.4	3.02	0.28	400	4.27	0.59	394	395
A^9(RI)	436.9	7.89	0.65	459	5.78	0.69	450	445
E_2^{10}(R)	445.1	7.15	0.58					
E_1^9(RI)	445.9	7.74	0.62					
E_2^{11}(R)	619.8	-1.40	-0.08					
E_1^{10}(RI)	622.1	-0.65	-0.04	685	-0.20	-0.02	685	685
A^{10}(RI)	637.7	-1.68	-0.09	703	-2.32	-0.18		
E_2^{12}(R)	674.7	0.07	0.00	727	-0.87	-0.07	726	726
E_1^{11}(RI)	697.9	-2.38	-0.12	765	-3.72	-0.27	755	756
A^{11}(RI)	729.2	-1.45	-0.07	792	-3.51	-0.24	795	796
E_1^{12}(RI)	770.7	-5.59	-0.26	821	-3.40	-0.23		826
A^{12}(RI)	774.0	-6.95	-0.32	829	-6.41	-0.43	831	
E_2^{13}(R)	791.1	-5.25	-0.24					

[a] This work, [b] Ref. 9, [c] Ref. 8

Figure Captions

Figure 1: Schematic representation of the crystal structure of $Fe(IO_3)_3$ at room pressure. Two different perspectives are shown. FeO_6 octahedral units are shown in brown color. I and O atoms are represented in purple and red color, respectively. Short I-O bonds are shown with gray solid lines, while long I-O bonds that do not result in an increased coordination are shown with blue dashed lines. Fe atoms are six-fold coordinated whereas I atoms are three-fold coordinated.

Figure 2: Selection of Raman spectra measured in $Fe(IO_3)_3$ at different pressures. The top Raman spectrum was taken upon decompression "d" to show the reversibility of the process. Bottom marks indicate the frequencies of the experimental modes at the smallest pressure.

Figure 3: Experimental (symbols) and theoretical (solid lines) pressure dependence of Raman-active mode frequencies in $Fe(IO_3)_3$. Green, black, and red colors correspond to A, E_1, and E_2 modes, respectively. In the high-frequency region (top panel), calculated modes have been shifted 60 cm^{-1} to higher frequencies to facilitate comparison with experiments. The vertical dashed lines indicate the pressures where changes associated to the two IPTs can be observed.

Figure 4: Calculated pressure dependence of I-O bond distances. The vertical dashed lines indicate the pressures where changes associated to the two IPTs can be observed. A gradual increase of I coordination can be inferred from this figure.

Figure 5: Theoretical $\omega^{-2/3}$ versus average theoretical I-O bond distances in IO_3 units of $Fe(IO_3)_3$. In the upper axis the pressure of each average bond distance is indicated. It can be seen that the average I-O bond distance increases under compression.

Figure 6: Calculated pressure dependence of elastic constants in $Fe(IO_3)_3$. The vertical dashed lines indicate the pressures where changes due to the two IPTs can be observed. Note the changes of the elastic constants especially around 1.5 GPa.

Figure 7: Calculated phonon dispersion curves along the Γ-M-K-Γ-A-L-H-Γ direction at 0 (a), 1.5 (b), 5.7 (c) and 7.5 GPa (d). At 1.5 and 5.7 GPa, small dynamic instabilities (smaller at 1.5 GPa) are observed near the Γ point that are not observed at 0 and 7.5 GPa.

Figure 8: Pressure dependence of the Full width at half maximum (FWHM) of phonons with frequency 400 and 792 cm^{-1}.

Figure 1

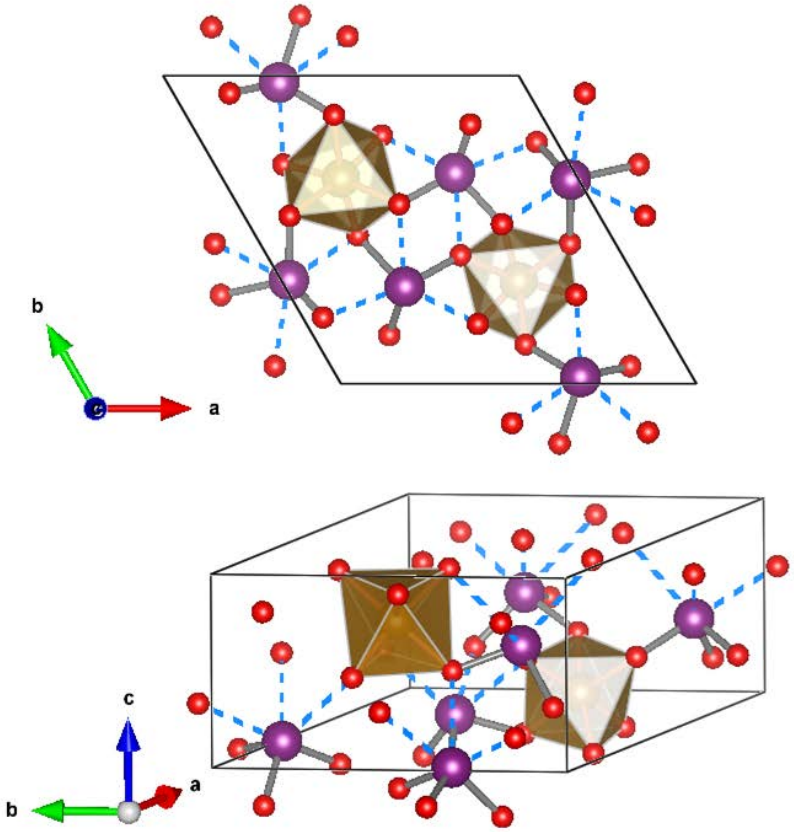

Figure 2

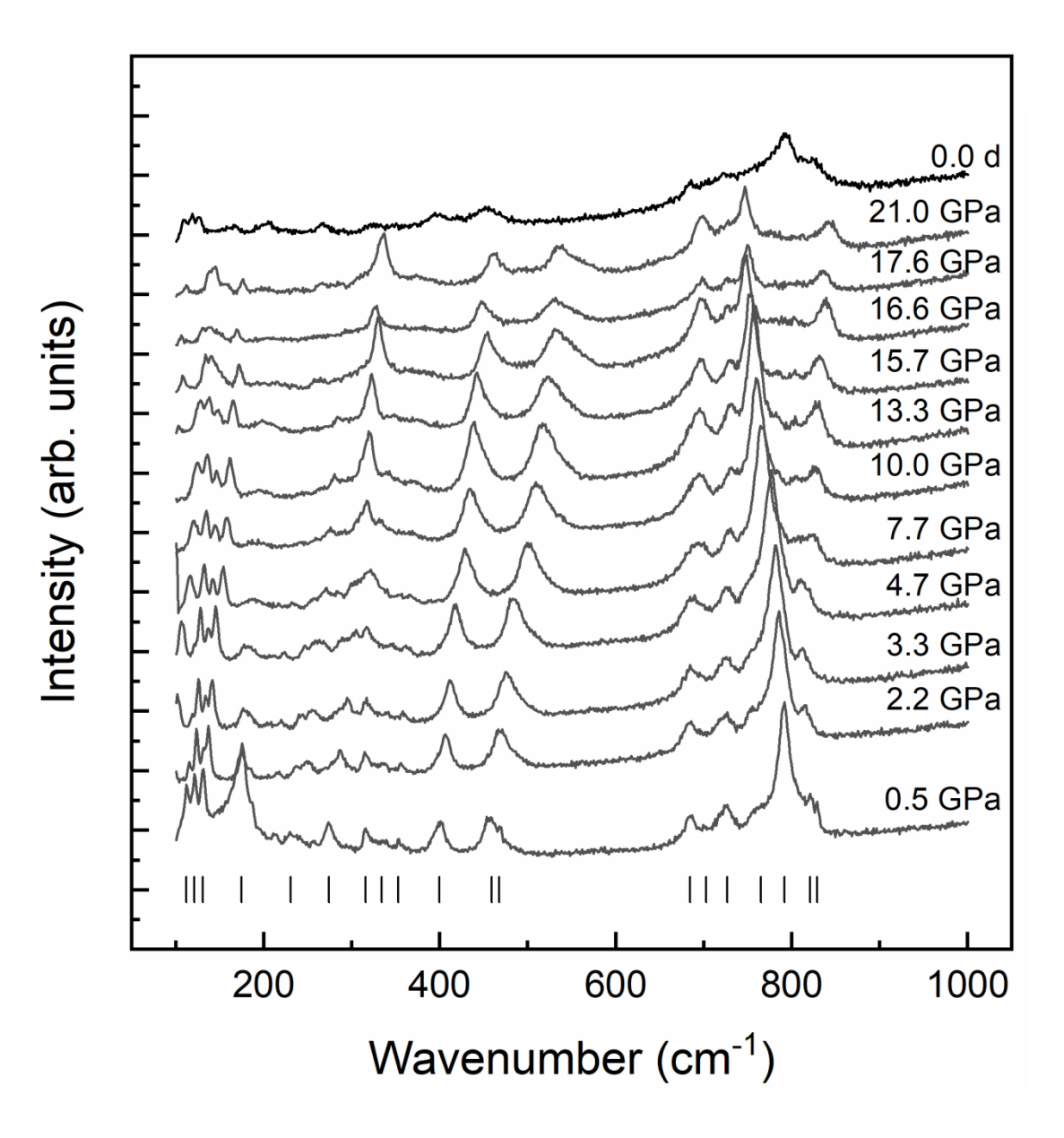
0.0 d
21.0 GPa
17.6 GPa
16.6 GPa
15.7 GPa
13.3 GPa
10.0 GPa
7.7 GPa
4.7 GPa
3.3 GPa
2.2 GPa
0.5 GPa
Intensity (arb. units)
200
400
600
800
1000
Wavenumber (cm-1)

Figure 3

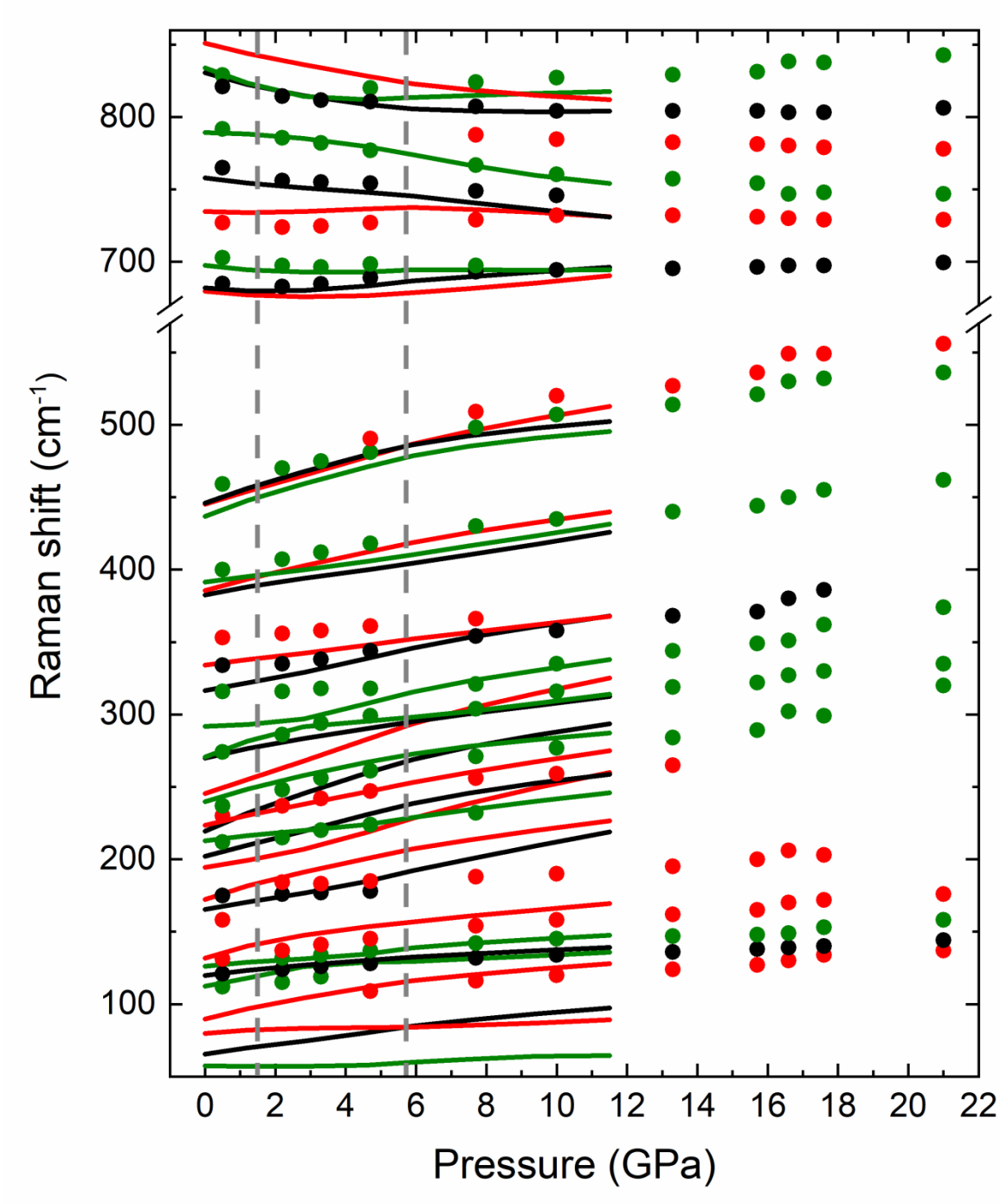
Raman shift (cm-1)
Pressure (GPa)
800
700
500
400
300
200
100
0
2
4
6
8
10
12
14
16
18
20
22

Figure 4

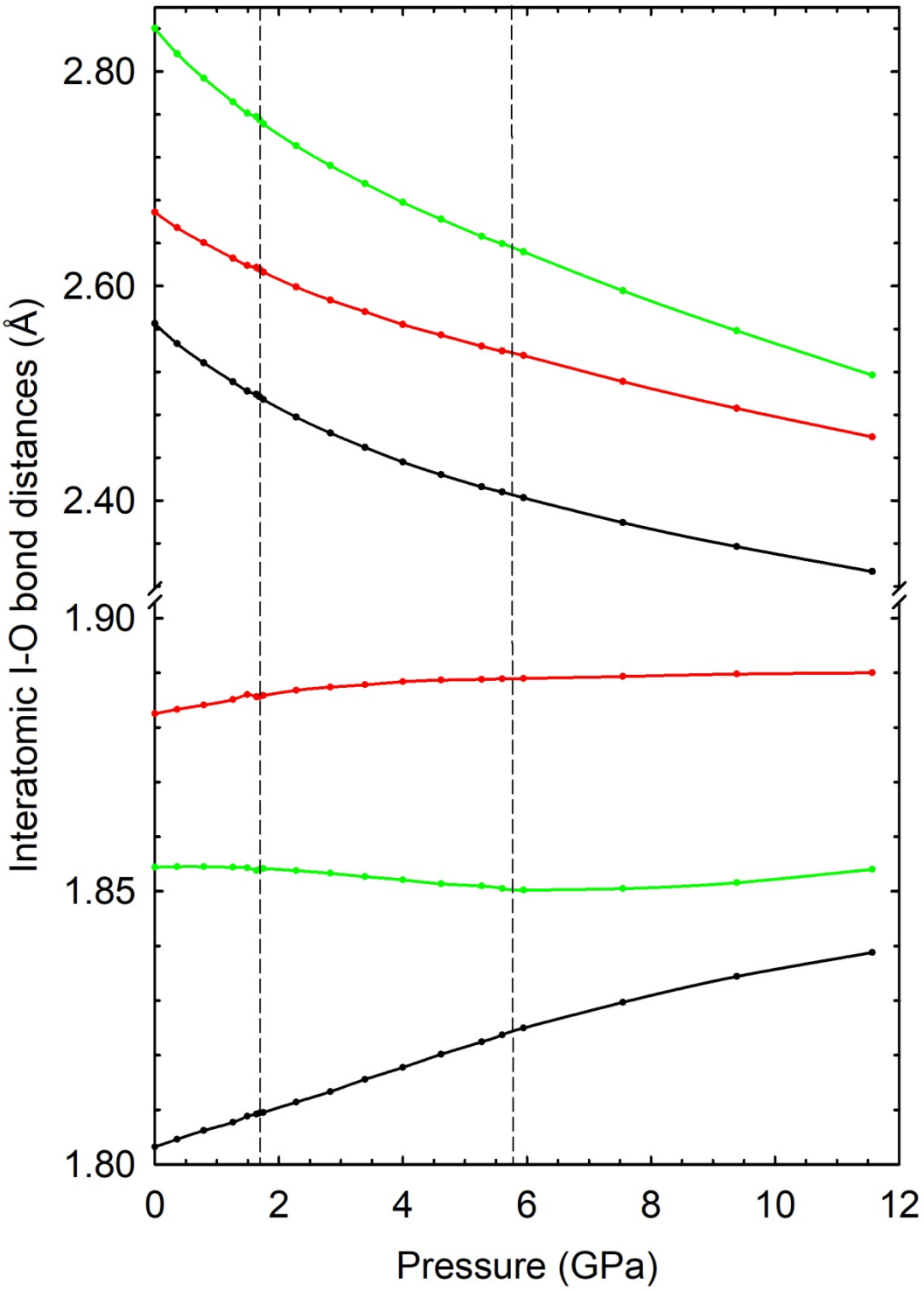
Interatomic I-O bond distances (Å)
2.80
2.60
2.40
1.90
1.85
1.80
0
2
4
6
8
10
12
Pressure (GPa)

Figure 5

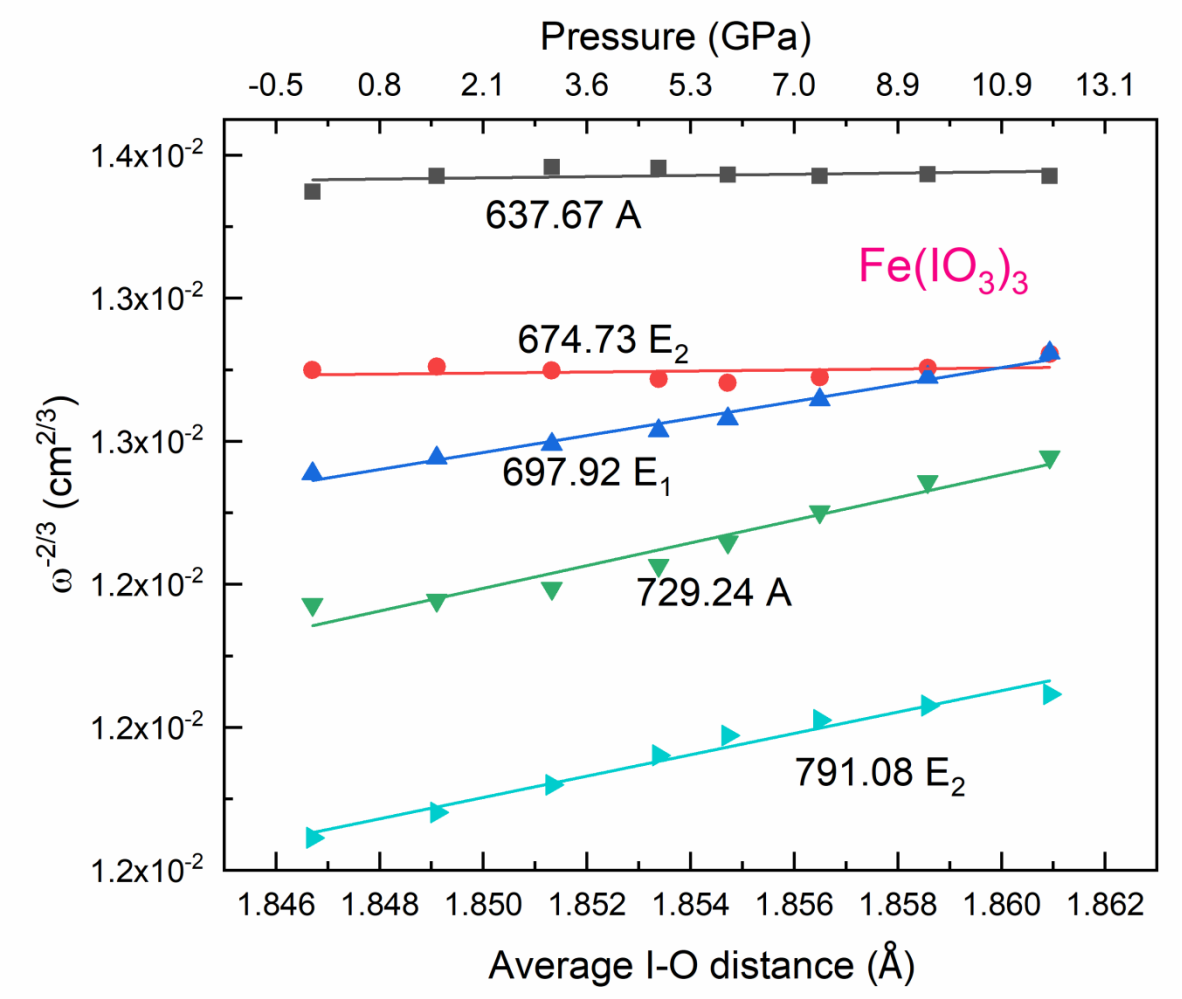
Pressure (GPa)
-0.5
0.8
2.1
3.6
5.3
7.0
8.9
10.9
13.1
1.4x10-2
1.3x10-2
1.3x10-2
1.2x10-2
1.2x10-2
1.2x10-2
ω-2/3 (cm2/3)
637.67 A
Fe(IO3)3
674.73 E2
697.92 E1
729.24 A
791.08 E2
1.846
1.848
1.850
1.852
1.854
1.856
1.858
1.860
1.862
Average I-O distance (Å)

Figure 6

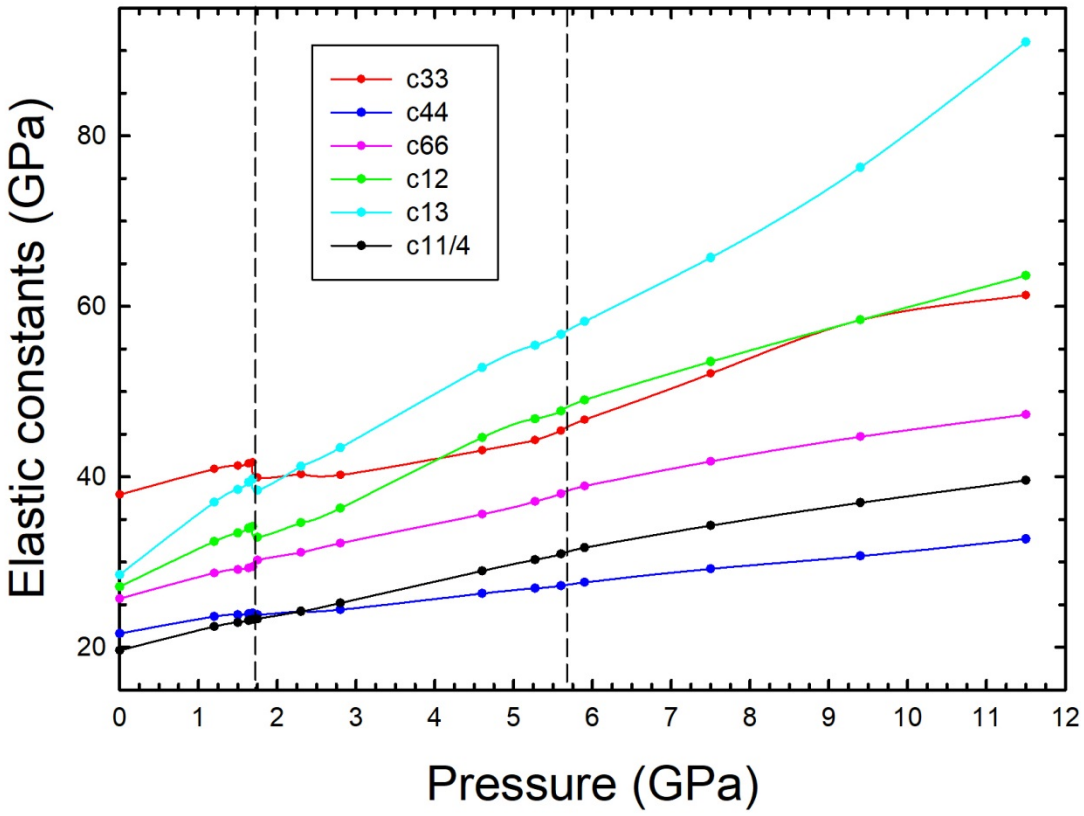
c33
c44
c66
c12
c13
c11/4
Elastic constants (GPa)
Pressure (GPa)
20
40
60
80
0
1
2
3
4
5
6
7
8
9
10
11
12

Figure 7

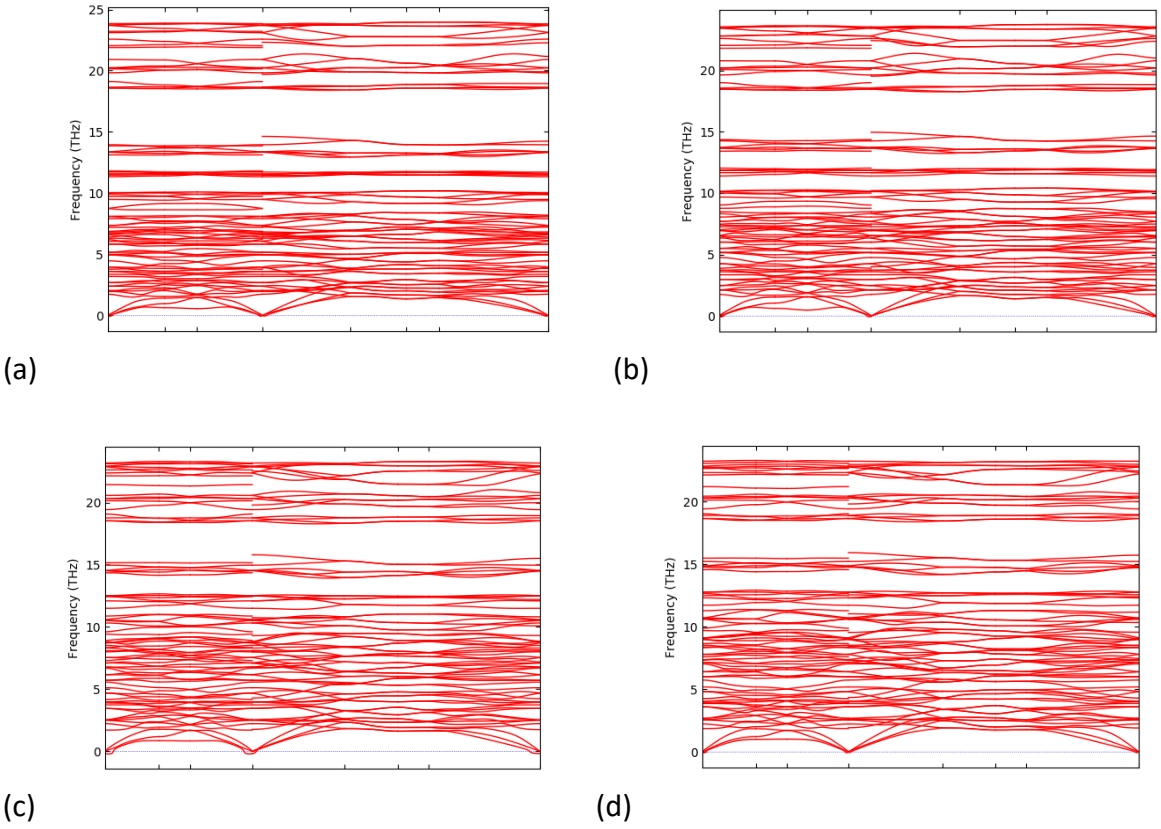

Figure 8

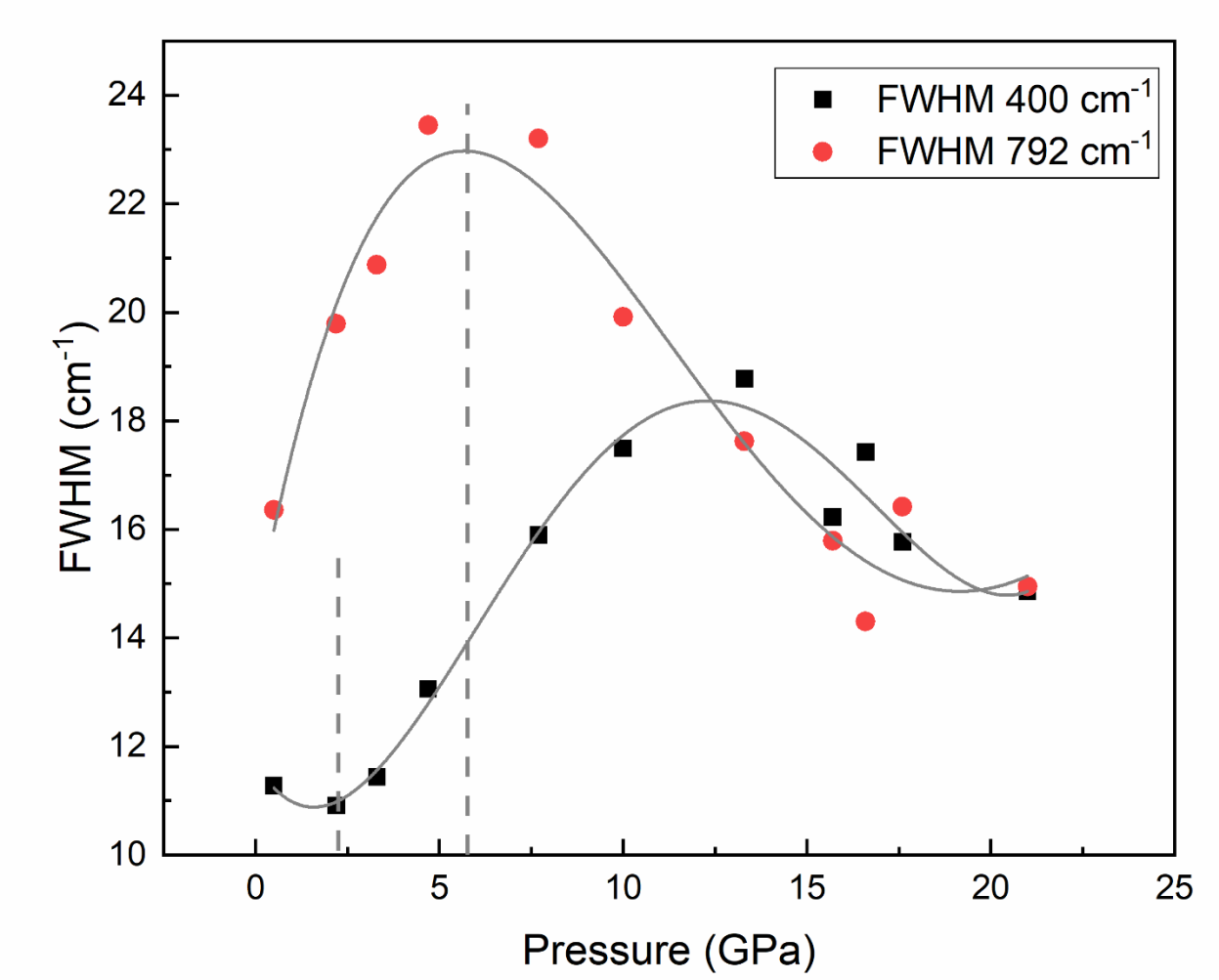
FWHM 400 cm-1
FWHM 792 cm-1
FWHM (cm-1)
Pressure (GPa)
24
22
20
18
16
14
12
10
0
5
10
15
20
25

Supplementary Material of High-pressure Raman study of $Fe(IO_3)_3$: Soft-mode behavior driven by coordination changes of iodine atoms

Akun Liang[1], Saqib Rahman[2], Placida Rodriguez-Hernandez[3], Alfonso Muñoz[3], Francisco Javier Manjón[4], Gwilherm Nenert[5], and Daniel Errandonea[1]

[1]Departamento de Física Aplicada - ICMUV - MALTA Consolider Team, Universitat de València, c/Dr. Moliner 50, 46100 Burjassot (Valencia), Spain

[2]Center for High Pressure Science and Technology Advanced Research, Shanghai 201203, China

[3]Departamento Física, Malta Consolider Team, and Instituto de Materiales y Nanotecnología, Universidad de La Laguna, 38206 La Laguna, Tenerife, Spain

[4]Instituto de Diseño para la Fabricación y Producción Automatizada, MALTA-Consolider Team, Universitat Politècnica de València, 46022 Valencia, Spain

[5]Malvern Panalytical B.V., Lelyweg 1, 7602 EA Almelo, The Netherlands

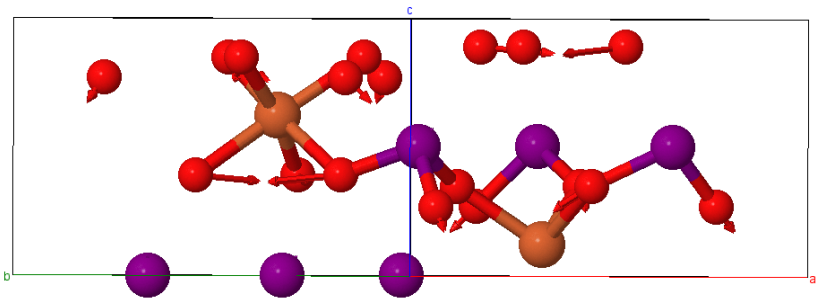

Figure S1: View of the atomic vibrations of the A^{11} mode of $Fe(IO_3)_3$ calculated at 729.2 cm^{-1} and corresponding to the experimental mode of 792 cm^{-1}. Orange, purple and red balls represent Fe, I and O atoms, respectively. This mode is a symmetric stretching I-O mode where the three O atoms of IO_3 units vibrate in-phase against the iodine atom.

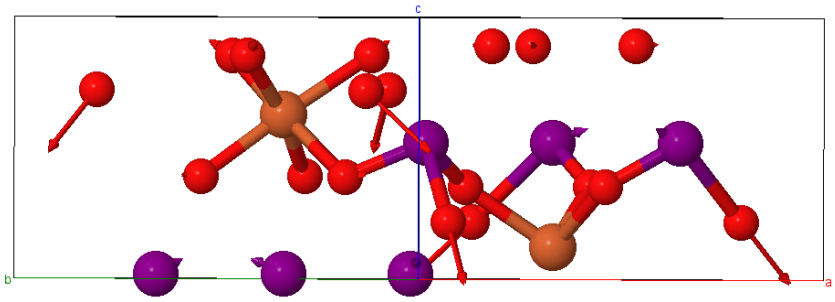

Figure S2: View of the atomic vibrations of the A^{12} mode of $Fe(IO_3)_3$ calculated at 774.0 cm^{-1} and corresponding to the experimental mode of 821 cm^{-1}. Orange, purple and red balls represent Fe, I and O atoms, respectively. This mode is an asymmetric stretching I-O mode where the one of the O atoms of IO_3 units vibrate against the iodine atom, while the other two O atoms are almost at rest.

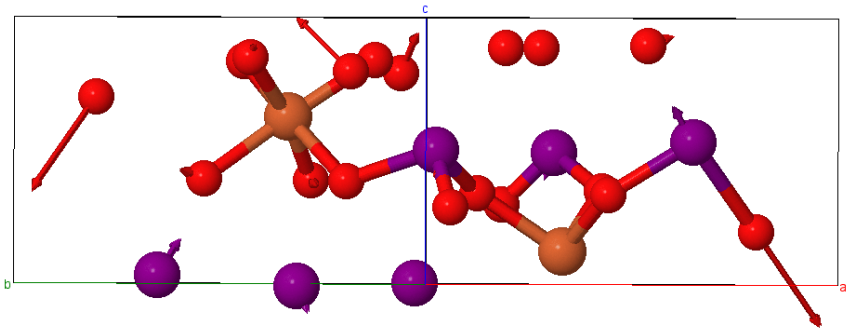

Figure S3: View of the atomic vibrations of the E_2^{13} mode of $Fe(IO_3)_3$ calculated at 791.1 cm^{-1} and corresponding to the experimental mode of 829 cm^{-1}. Orange, purple and red balls represent Fe, I and O atoms, respectively. This mode is an asymmetric stretching I-O mode where the one of the O atoms of IO_3 units vibrate against the iodine atom, while the other two O atoms are almost at rest. Note the different small movement of I atoms in this mode and in the A^{12} mode.

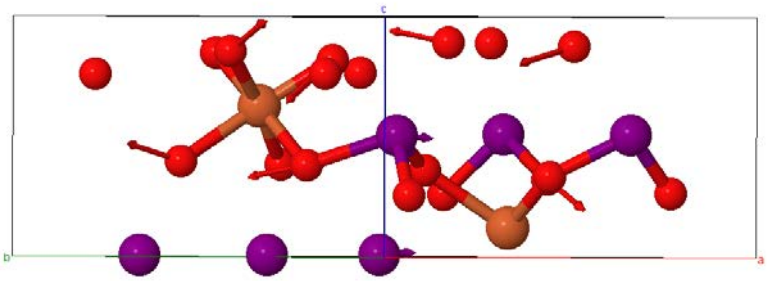

Figure S4: View of the atomic vibrations of the E_1^{10} mode of $Fe(IO_3)_3$ calculated at 622.1 cm^{-1} and corresponding to the experimental mode of 685 cm^{-1}. Orange, purple and red balls represent Fe, I and O atoms, respectively. This mode is another asymmetric stretching I-O mode where the two of the O atoms of IO_3 units vibrate out-of-phase against the I atom, while the other O atom is almost at rest.

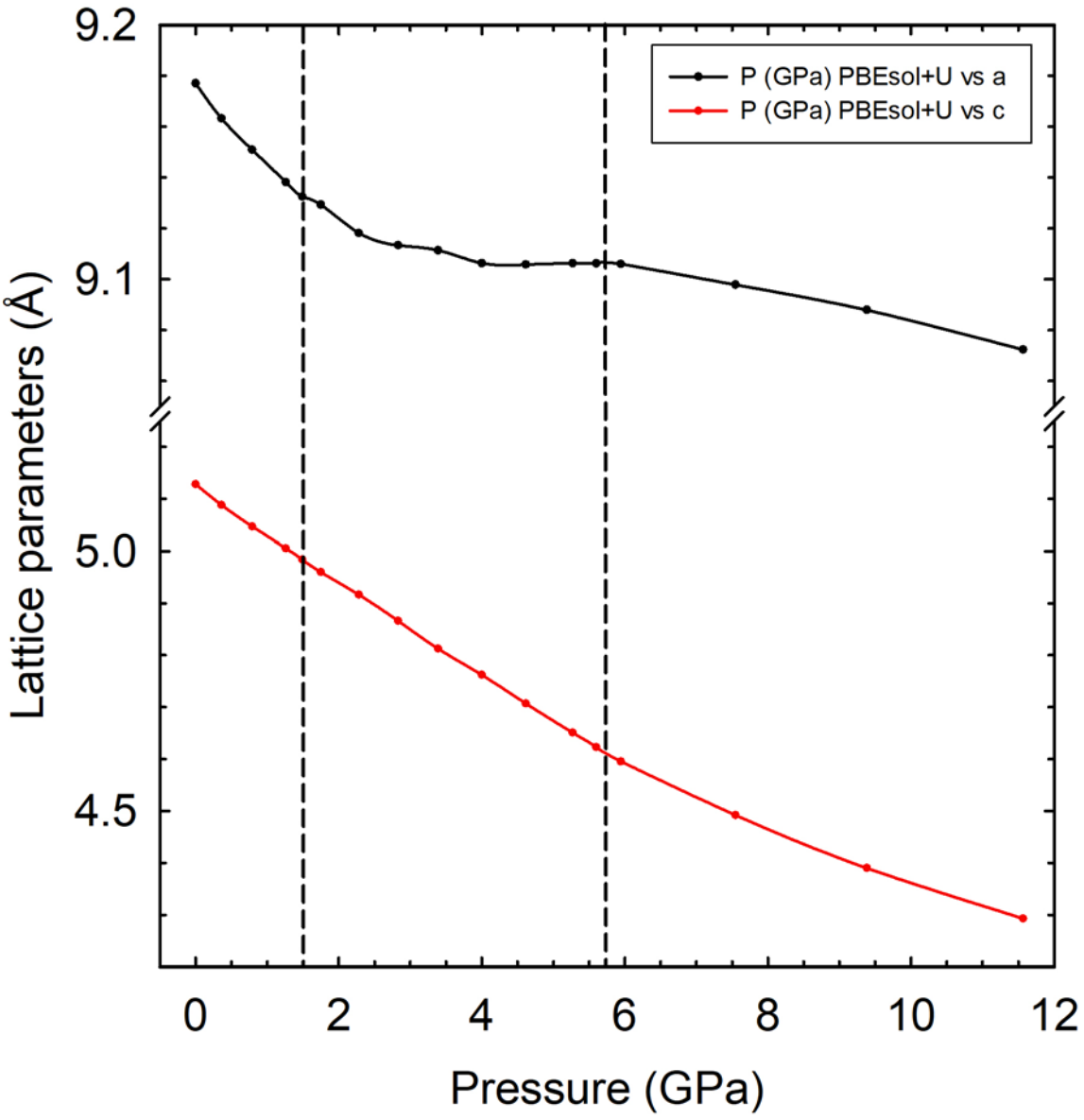

Figure S5: Calculated pressure dependence of lattice parameters a and c in $Fe(IO_3)_3$. The vertical dashed lines indicate the pressures where changes associated to the IPTs can be observed.

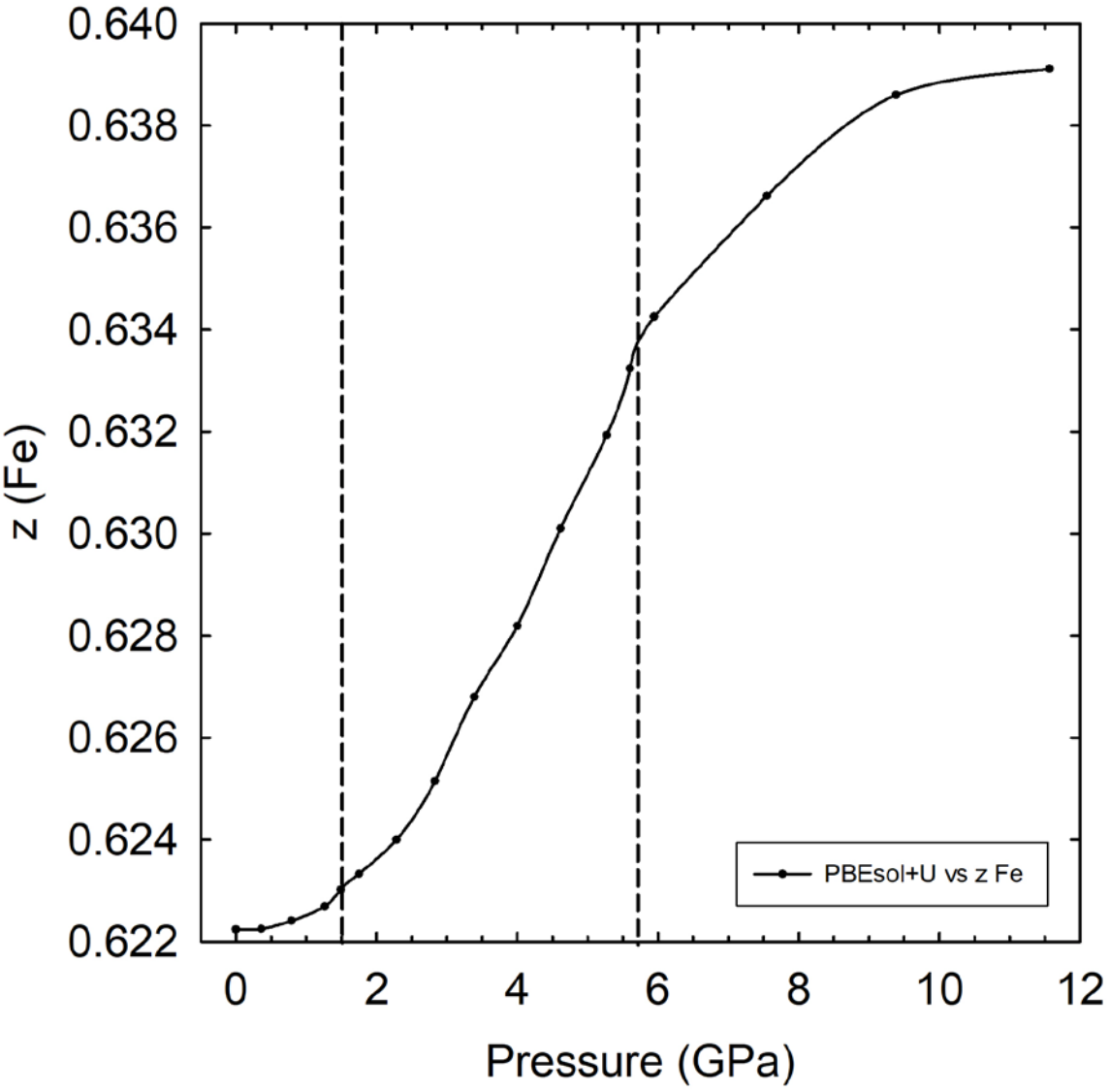

Figure S6: Calculated pressure dependence of z free atomic parameter of the Fe atom in $Fe(IO_3)_3$. The vertical dashed lines indicate the pressures where changes associated to the IPTs can be observed. Note the S-like behavior of this free atomic parameter.

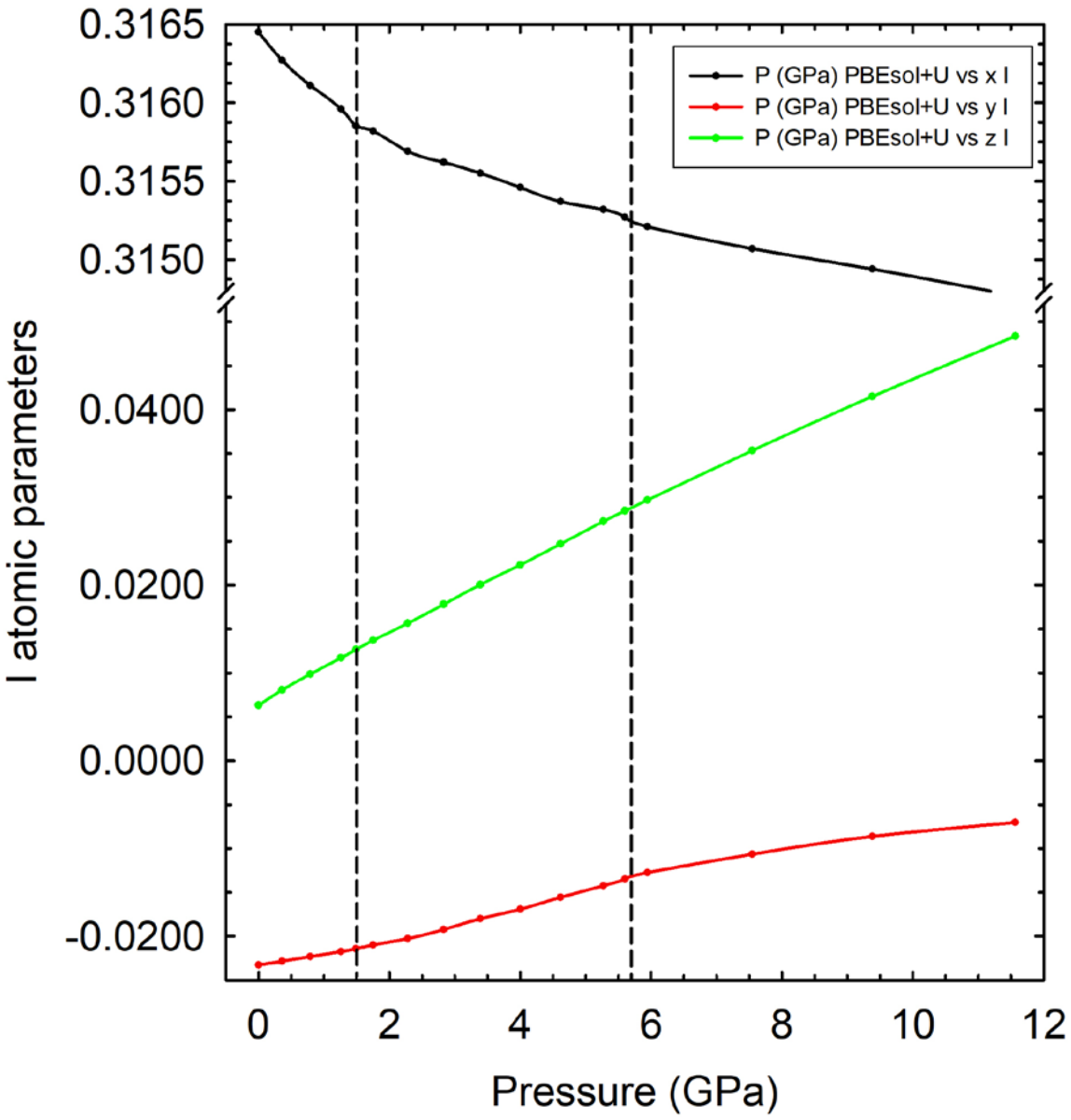

Figure S7: Calculated pressure dependence of x, y, and z free atomic parameters of the I atom in $Fe(IO_3)_3$. The vertical dashed lines indicate the pressures where changes associated to the IPTs can be observed. Note the S-like behavior of the y free atomic parameter.

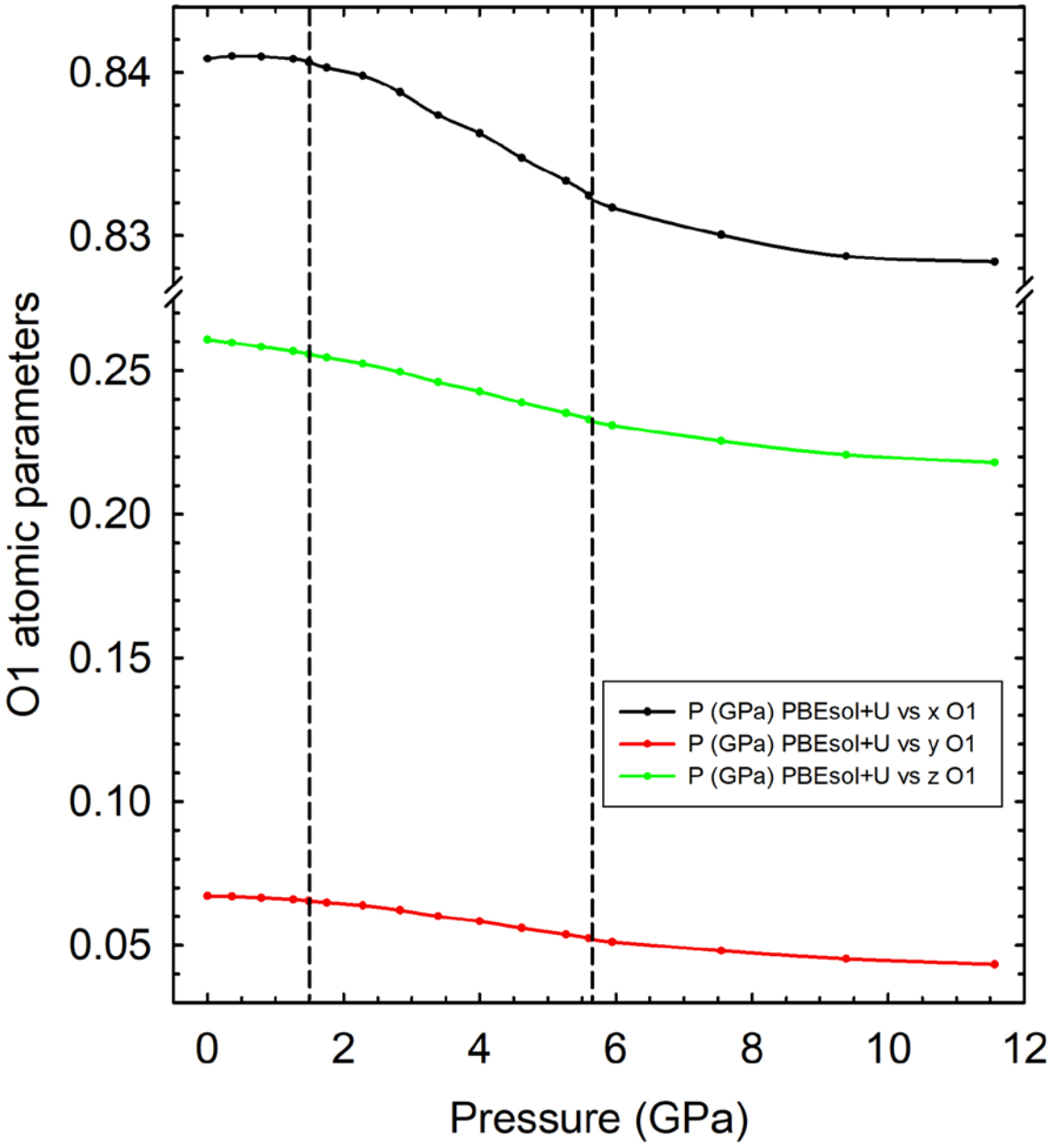

Figure S8: Calculated pressure dependence of x, y, and z free atomic parameters of the O1 atom in $Fe(IO_3)_3$. The vertical dashed lines indicate the pressures where changes associated to the IPTs can be observed. Note the S-like behavior of the three free atomic parameters.

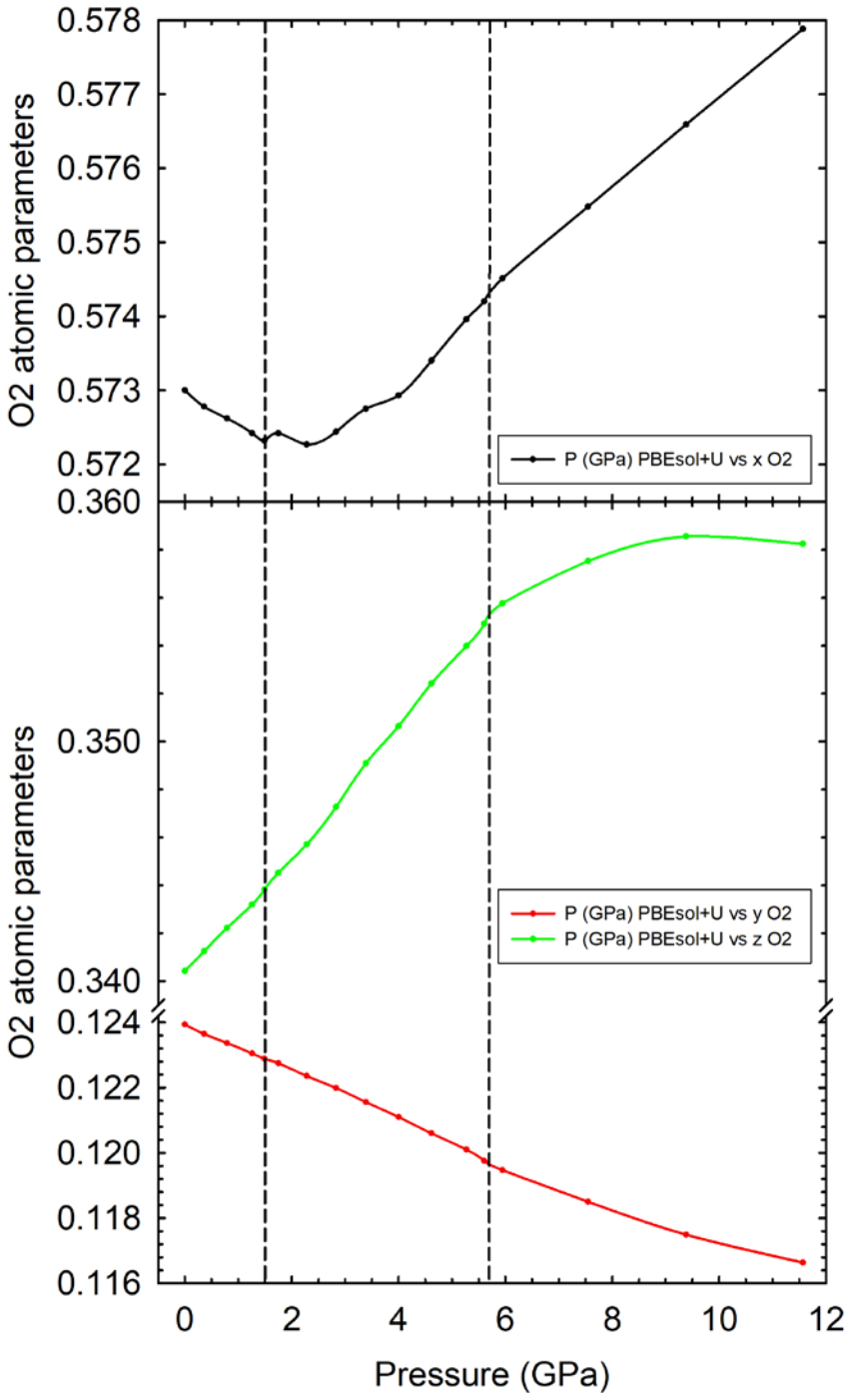

Figure S9: Calculated pressure dependence of x, y, and z free atomic parameters of the O2 atom in $Fe(IO_3)_3$. The vertical dashed lines indicate the pressures where changes associated to the IPTs can be observed. Note the completely different behavior of the three free atomic parameters in the three pressure regions.

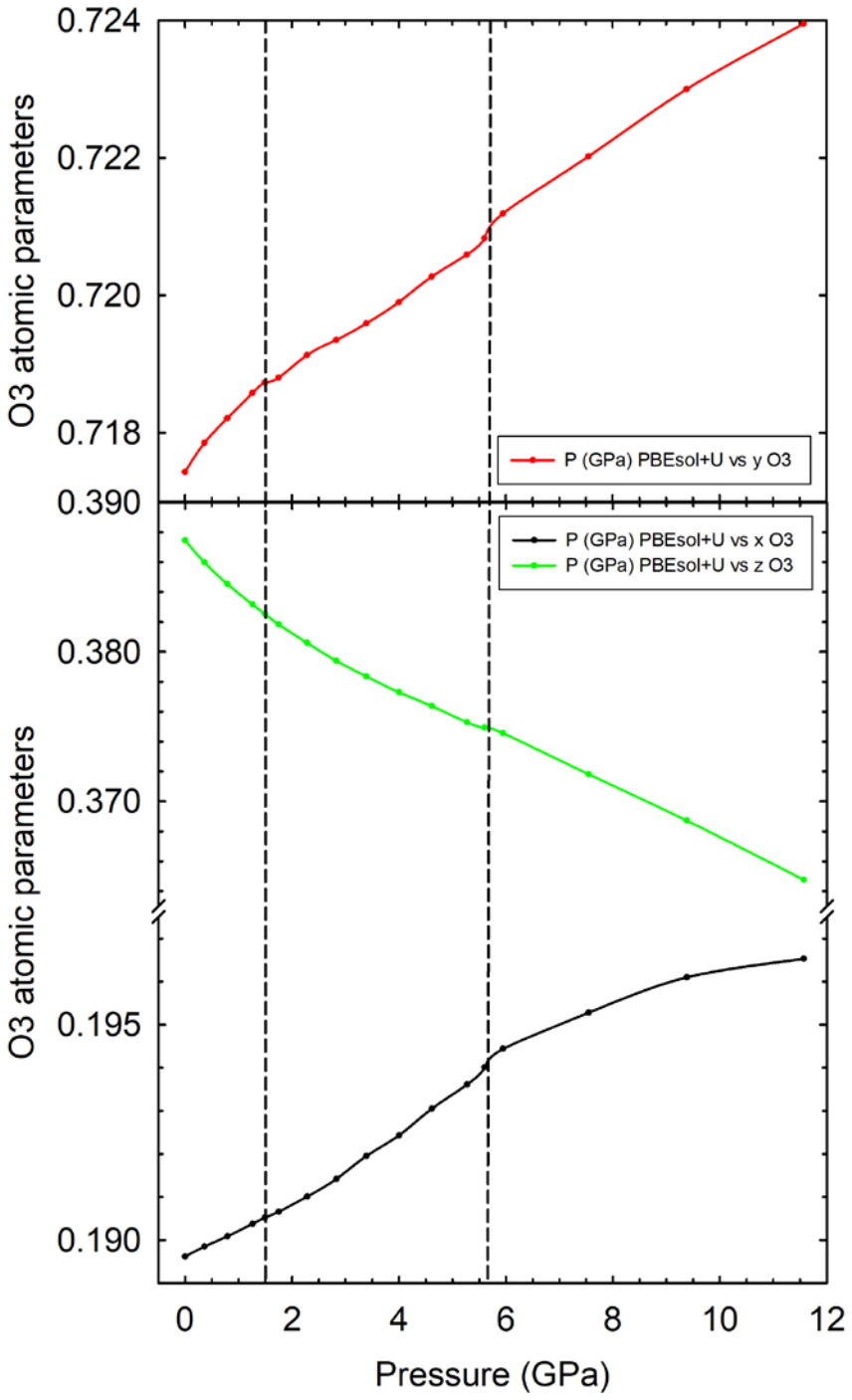

Figure S10: Calculated pressure dependence of x, y, and z free atomic parameters of the O3 atom in $Fe(IO_3)_3$. The vertical dashed lines indicate the pressures where changes associated to the IPTs can be observed. Note the completely different behavior of the three free atomic parameters in the three pressure regions.